This is a repository copy of *Remote functionalization in surface-assisted dehalogenation by conformational mechanics: organometallic self-assembly of 3,3′,5,5′-tetrabromo-2,2′,4,4′,6,6′-hexafluorobiphenyl on Ag(111)*.

White Rose Research Online URL for this paper:
http://eprints.whiterose.ac.uk/132411/

Version: Accepted Version

Journal Name

ARTICLE

Remote functionalization in surface-assisted dehalogenation by conformational mechanics:
organometallic self-assembly of 3,3',5,5'-tetrabromo-2,2',4,4',6,6'-hexafluorobiphenyl on Ag(111)

Matthias Lischka,[a,b] Georg S. Michelitsch,[c] Natalia Martsinovich,[d] Johanna Eichhorn,[a,b] Atena Rastgoo-Lahrood,[a,b] Thomas Strunskus,[e] Rochus Breuer,[f] Karsten Reuter,[c] Michael Schmittel,[f] and Markus Lackinger [*,a,b,g]

Even though the surface-assisted dehalogenative coupling constitutes the most abundant protocol in on-surface synthesis, its full potential will only become visible if selectivity issues with polybrominated precursors are comprehensively understood, opening new venues for both organometallic self-assembly and surface polymerization. Using the 3,3',5,5'-tetrabromo-2,2',4,4',6,6'-hexafluorobiphenyl (Br_4F_6BP) at Ag(111), we demonstrate a remote site-selective functionalization at room temperature and a marked temperature difference in double- *vs.* quadruple activation, both phenomena caused by conformational mechanical effects of the precursor-surface ensemble. The submolecularly resolved structural characterization was achieved by Scanning Tunneling Microscopy, the chemical state was quantitatively assessed by X-ray Photoelectron Spectroscopy, and the analysis of the experimental signatures was supported through first-principles Density-Functional Theory calculations. The non-planarity of the various structures at the surface was specifically probed by additional Near Edge X-ray Absorption Fine Structure experiments. Upon progressive heating, Br_4F_6BP on Ag(111) shows the following unprecedented phenomena: (1) formation of regular organometallic 1D chains via remote site-selective 3,5'didebromination; (2) a marked temperature difference in double- vs quadruple activation; (3) an organometallic self-assembly based on reversibility of C-Ag-C linkages with a thus far unknown polymorphism affording both hexagonal and rectangular 2D networks; (4) extraordinary thermal stability of the organometallic networks. Defined covalent coupling was not achieved for the Br_4F_6BP precursor, but only for the comparitively studied non-fluorineted analogue.

Introduction

Over the last decade, the bottom-up fabrication of metal-organic and covalent nanostructures on solid surfaces has gained significant interest and momentum.[1-4] The main idea and benefit of such on-surface synthesis are to combine the stability gained by strong interlinks with the versatility of molecular systems. This approach afforded an intriguing variety of atom-precise structures, comprising covalent 1D wires, chains, and ribbons, as well as 2D networks including first steps towards electronic conjugation.[5, 6] For metal-organic networks the chemical structure of the ligands and choice of coordination centers both facilitate tuning and tailoring of network topologies and properties. In this respect, the introduction of iron or cobalt as coordination center promises unsurpassed catalytic or magnetic properties.[7, 8] Moreover, recently unique 5-fold coordination motifs were realized in a 2D environment using rare-earth metals, even resulting in networks with quasicrystalline characteristics.[9] An intriguing variant are the organometallic structures based on carbon-metal-carbon linkages that are routinely observed as metastable intermediates on silver and copper surfaces upon dissociation of halogen substituents that act as leaving groups. Both metal-organic and organometallic linkages can become reversible, as important premise for self-assembly of highly ordered networks.[10] Moreover, structural equilibration in organometallic networks represents a viable route to improve the structural quality of the corresponding covalent networks that are obtained through a thermally activated isostructural

a. Department of Physics, Technische Universität München, James-Frank-Str. 1, 85748 Garching, Germany. E-mail: markus@lackinger.org
b. Center for NanoScience (CENS) & Nanosystems-Initiative-Munich, Schellingstr. 4, 80799 München, Germany
c. Chair for Theoretical Chemistry and Catalysis Research Center, Technische Universität München, Lichtenbergstraße 4, 85747 Garching, Germany
d. Department of Chemistry, University of Sheffield, Sheffield S3 7HF, U.K.
e. Institute of Materials Science – Multicomponent Materials, Christian-Albrecht-Universität zu Kiel, Kaiserstr. 2, 24143 Kiel, Germany
f. Center of Micro- and Nanochemistry and Engineering, Organische Chemie I, Universität Siegen, Adolf-Reichwein-Str. 2, 57068 Siegen, Germany
g. Deutsches Museum, Museumsinsel 1, 80538 Munich, Germany
† Electronic Supplementary Information (ESI) available: additional STM &XPS data; additional DFT simulations; synthesis details; See DOI: 10.1039/x0xx00000x

conversion.[11-14] Yet, inducing reversibility in organometallic bonds typically requires higher temperatures as compared to their metal-organic counterparts. In general, the surface-templated bottom-up synthesis of 2D materials with unprecedented chemical, structural, and electronic properties is highly inspiring for nanotechnological applications in a broad variety of fields such as electronics, sensors, separation, and catalysis.[15, 16]

In principle, on-surface synthesis facilitates reticular design of novel 2D materials, predetermining arbitrary ordered structures through the judicious choice of the assembling molecular units. However, limited regioselectivity, side reactions, surface influence, and the absence of error correction due to the irreversibility of newly established covalent links render this conceptually straightforward approach challenging in practice. In this respect, well-behaved and controllable coupling reactions for fusing the molecular units are of crucial importance. To date, surface-assisted Ullmann coupling is the most reliable and predictable workhorse to achieve linking *via* C-C bonds,[17] which furthermore benefits from the abundant availability of the employed halogenated precursors. Ullmann coupling is based on aryl halides that can easily be dissociated on metal surfaces, in most cases Cu, Ag, or Au. The generated surface-stabilized radicals may subsequently recombine to form new C-C linkages, either directly or *via* metastable organometallic intermediates.[14, 18] Consequently, research on organometallic self-assembly was initially fueled by the large interest in on-surface synthesis of covalent nanostructures, but has now become a topic of its own.
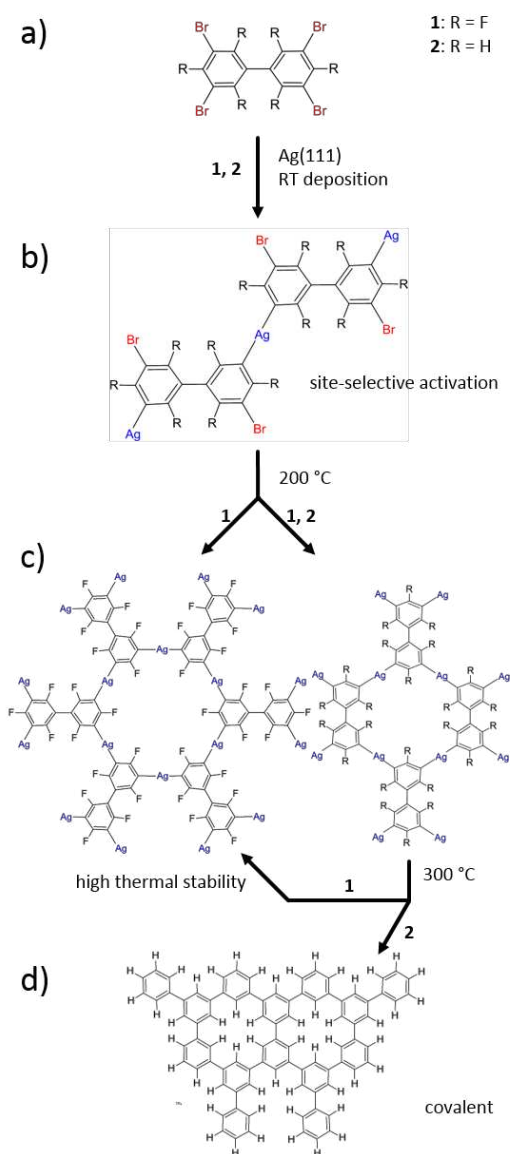
Despite this relevance and significant research efforts into the dehalogenation as the preceding step for both organometallic self-assembly and Ullmann coupling, many central issues of reactivity, chemo- and regioselectivity are still poorly understood. For instance, 1,3-bis(*p*-bromophenyl)-5-(*p*-iodophenyl)benzene showed full deiodination and ~38% debromination after room temperature deposition onto Ag(111), but debromination was only completed at ~260 °C.[14] In stark contrast, 1,3,5-tris(*p*-bromophenyl) benzene was not debrominated at all after room temperature deposition onto Ag(111), but already fully debrominated upon annealing to ~120 °C.[19] Such examples of differential reactivity highlight the current lack of understanding, which prevents a higher level of control in on-surface synthesis that is an absolute necessity for improving the notoriously low structural qualities, currently the most crucial hindrance for applications.

Here we address the reactivity as well as chemo- and regioselectivity of surface-assisted debromination in 3,3',5,5'-tetrabromo-2,2',4,4',6,6'-hexafluorobiphenyl (Br$_4$F$_6$BP, cf. Fig. 1(a) for its structure) as a prototypical representative of a perfluorinated oligobromoarene. Fluorine substitution constitutes an important strategy to chemically alter relevant properties of neighbouring groups and is additionally expected to influence formation, reversibility, and stability of

organometallic networks. In general, fluorination enhances the electron acceptor properties, and attractive electronic properties were predicted for edge-fluorinated graphene nanoribbons.[20, 21]

We explore the thermally activated surface chemistry of Br$_4$F$_6$BP by a multi-technique approach, comprising a deep structural, chemical, and first-principles computational characterization. The bond dissociation energy of F-C in the gas phase of 5.4 eV even exceeds the value of 5.1 eV for C-C bonds, suggesting that activation of the fluorinated sites is rather unlikely, even if the proximity of a surface can promote defluorination.[22, 23] Given the high volatility of Br$_4$F$_6$BP, the more reactive Ag(111) surface was chosen, as thermally activated surface chemistry is not feasible on more noble Au(111) surfaces due to preferential desorption of the precursors upon heating (cf. ESI). The key findings for Br$_4$F$_6$BP and its comparatively studied non-fluorinated analogue 3,3',5,5'-tetrabromo-biphenyl (Br$_4$BP) on Ag(1111) are summarized in Fig. 1

Fig. 1 Overview over the thermally induced structural and chemical changes of Br$_4$F$_6$BP and Br$_4$BP on Ag(111)

A priori, various effects of the perfluorination are conceivable: **(1)** The C-Br bond strength ought to be modified by inductive effects, resulting in altered debromination barriers/temperatures and reaction kinetics, respectively. By the same token, the strength of the C-Ag-C linkages in the organometallic intermediate could be altered. **(2)** The gas phase structure of Br_4F_6BP is highly non-planar with a large dihedral angle and rotational barrier at the biphenyl unit due to the *ortho*-fluorine substituents, which could have consequences for the surface chemistry and the regioselectivity of the second debromination step. **(3)** The *ortho*-fluorine atoms next to the reactive C-Br gives rise to an additional barrier for the covalent aryl-aryl coupling. **(4)** The high electronegativity of fluorine influences non-covalent intermolecular bonds that steer the organization of precursors as well as reaction intermediates and products. Direct effects are expected due to the negative partial charge, but fluorine substituents can also enhance the halogen bond strength of neighbouring bromine or iodine substituents,[24] or even directly form halogen bonds.[25]

Results

After room-temperature deposition (RT) of Br_4F_6BP onto Ag(111) two different structures were observed by Scanning Tunneling Microscopy (STM), representative images are depicted in Figs. 2(a) and (b) (cf. ESI for overview images). Evidently, the structure shown in Fig. 2(a) consists of interdigitated 1D chains. A perfect geometrical match is achieved with organometallic chains based on C-Ag-C linkages that result from exclusive didebromination of the precursors across the diagonal, i.e. at the 3- and 5'-positions. The bright protrusions on alternating sides of the chains are attributed to remaining bromine substituents at the 5- and 3'- positions. The experimentally determined repeat distance of (1.06 ± 0.10) nm is consistent with the DFT-derived value of 1.02 nm found for a periodic planar chain, excluding direct covalent bond formation that would result in a ~0.25 nm smaller value.[14]

Chain interdigitation is likely driven by weak halogen bonding between the remaining Br- and the F-substituents. The more regular and densely packed structure in Fig. 2(b) features an oblique unit cell with a = (1.06 ± 0.06) nm, b = (0.78 ± 0.08) nm, γ = 85°. Also this structure matches perfectly with organometallic chains, yet with a higher packing density. This assignment is corroborated by the equal repeat distance in chain direction (corresponding to lattice parameter a) and the pronounced STM contrast at the positions of the remaining bromine substituents. The average chain length in the less densely packed structure corresponds to (12.7 ± 11) nm and increases only slightly to (14.7 ± 13.6) nm for the more densely packed structure. These lengths were evaluated for domains with packed chains, ignoring the relatively short chain segments in more defective areas (cf. ESI).

The observed formation of organometallic structures agrees with previous studies of various brominated precursors on Ag,
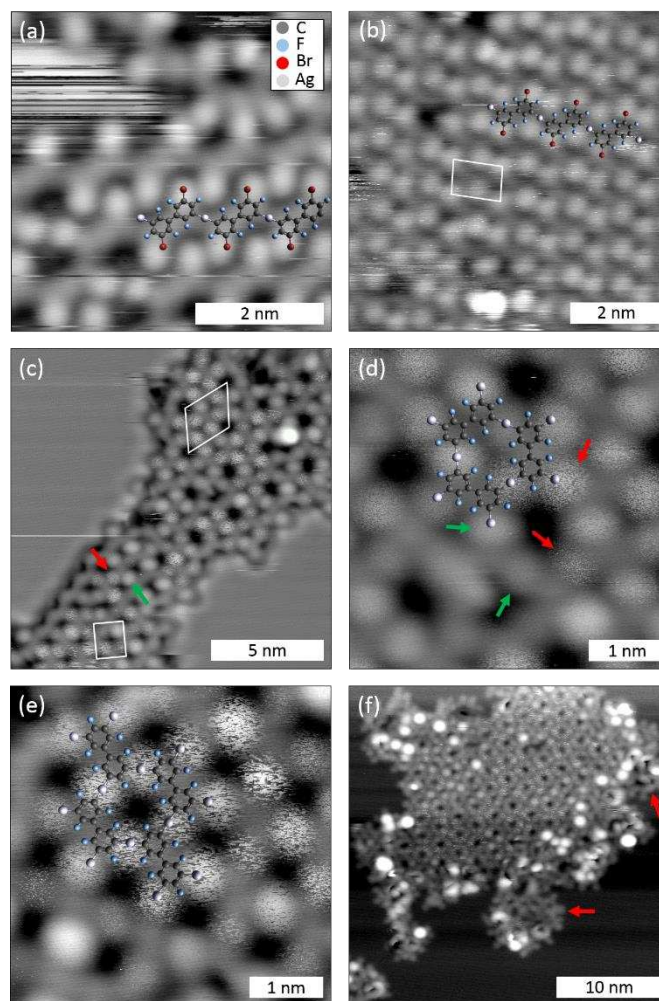

Fig. 2 STM images acquired (a) / (b) after RT deposition of Br4F6BP on Ag(111), and subsequent annealing to (c) − (e) 200 °C and (f) 300 °C. After RT deposition (a) more loosely and (b) densely packed ordered arrangements of organometallic chains were observed. Annealing to 200 °C resulted in coexisting organometallic flower ((c) overview, (d) close-up) and (e) checkerboard structures; (f) the flower structure persisted even after annealing to 300 °C. Unit cells are indicated by white lines ((a), (c)). Tunneling parameters: (a) 44 pA, -0.69 V; (b) 22 pA, 1.26 V; (c) 45 pA, 0.58 V; (d) 45 pA, 0.58 V; (e) 42 pA, 0.60 V; (f) 92 pA, 0.53 V. voltage polarities refer to the tip.

consistently reporting organometallic intermediates upon partial debromination at room temperature.[14, 18, 26, 27] Yet, an intriguing aspect here is the remote site-selective didebromination exclusively at the 3- and 5'-positions, as required for chain formation. To unveil structural details of the chains and also to explain the STM contrast, isolated chains were simulated either with enforced planar geometry or alternatively by constraining all Ag atoms to similar height. The latter conditions result in significant tilting of the phenyl rings in the biphenyl unit with a dihedral angle of ~49° and a slightly reduced repeat distance of 0.986 nm. Based on a comparison of the experimental STM images with the relatively pronounced contrast at the remaining bromine substituents and respective STM image simulations, better agreement is achieved for tilted than for planar chains (cf. ESI). Yet, the structure of adsorbed chains might become decisively modified through interactions with the surface. Therefore, additional DFT simulations were carried out including the Ag(111) surface (cf. ESI). Among the stable structures two

perfectly matching candidates were identified. Both structures feature a repeat distance of 1.05 nm along the chain, and interchain spacings of 0.77 nm and 1.05 nm, in accord with the experimental values of (0.78 ± 0.08) nm and (1.03 ± 0.10) nm for the more loosely and densely packed structures, respectively. Even in the presence of the surface, the biphenyl units remain significantly tilted, with large dihedral angles of ~58° and ~43° for the more densely and loosely packed structures. Consequently, the remaining bromine substituents also appear with a pronounced contrast in the corresponding STM image simulations (cf. ESI).

The proposed 3,5'-didebromination after room temperature deposition is also corroborated by the corresponding Br 3d X-ray Photoelectron (XP) spectrum in Fig. 3(b) showing two chemically shifted Br species, each appearing as a spin-orbit doublet. The species with a higher Br $3d_{5/2}$ binding energy (BE) of 70.2 eV corresponds to carbon-bound Br on the molecule,[26] whereas the species at a lower BE of 68.1 eV indicates surface-bound, i.e. dissociated bromine.[14, 18] Fitting results in a peak area ratio of ~65% molecule-bound and ~35% dissociated bromine. For perfect infinite chains, a debromination ratio of 50% is expected. Hence, the lower experimental value may indicate relatively short chains or other type of defects.

Fig. 3 XP spectra of C 1s (left column) and Br 3d (right column) acquired after RT deposition of Br_4F_6BP (upper row) and subsequent annealing at 200 °C (middle row) and 300 °C (lower row). Raw data are represented by dots; solid lines show fits with Gaussian line shape and linear background. C1s fits are assigned to following colour scheme: C-F(4,4'), dark cyan; C-F(2,6';2',6), light blue; C-Br, blue; C-C, green; C-Ag in half brominated and half organometallic phenyl rings, light pink; C-Ag in fully organometallic phenyl rings, magenta; Br 3d fits are presented for Br-C in blue and chemisorbed Br in green; red lines correspond to the sum of all components.
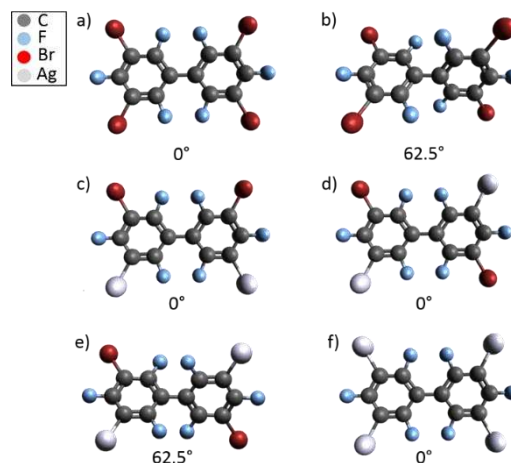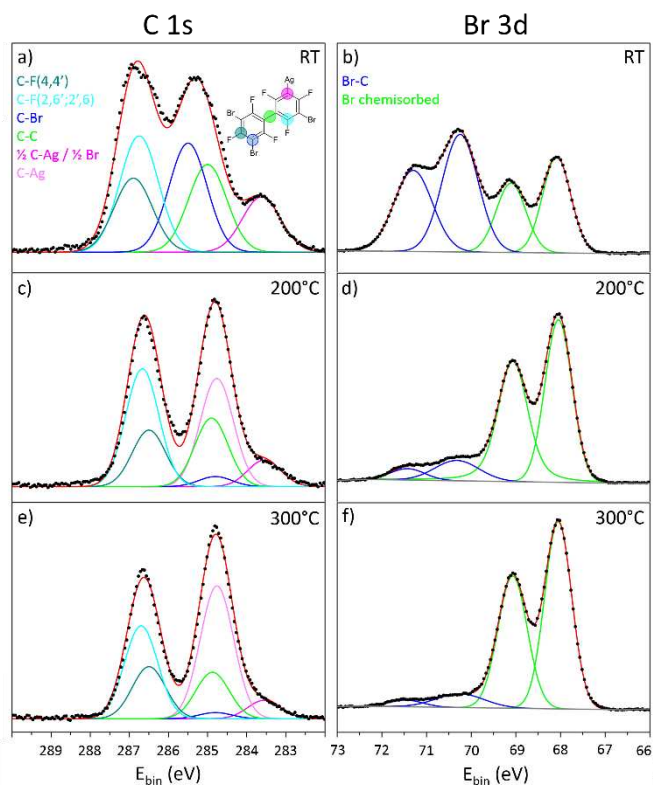

Fig. 4 Chemically distinct structures considered in the C 1s core-level shift simulations (the dihedral angles are indicated below): (a) fully brominated, planar; (b) fully brominated, non-planar with a dihedral angle of 62.5°; (c) 50 % debrominated, 50 % organometallic, cis, planar; (d) 50 % debrominated, 50 % organometallic, trans, planar; (e) 50 % debrominated, 50 % organometallic, trans, non-planar with a dihedral angle of 62.5°; (f) fully debrominated and organometallic, planar

The strong evidence for organometallic linkages from STM is further corroborated by the C 1s XP spectrum in Fig. 3(a). As a guideline for the fitting of this rather complex C 1s spectrum with contributions from carbon atoms in various different chemical environments, core-level shifts were calculated for isolated species by DFT. The simulations were carried out on each symmetry-inequivalent carbon atom one at a time. All structures considered are depicted in Fig. 4, and the calculated core-level shifts are summarized in Table 1, where intact precursors are also included for comparison. Irrespective of the exact configuration, the following common features of the core-level shifts are identified: As anticipated, the fluorine-substituted carbons (C-F) exhibit the highest C 1s BEs in accord with literature.[28, 29] Additional small relative shifts can occur at the non-equivalent positions. In contrast, the organometallic carbon atoms directly bound to Ag (C-Ag) always appear at the lowest BE. Interestingly, the relative order of C 1s BEs of the 1 / 1' carbons (C-C) at the linkage of the two phenyl units and bromine-substituted (C-Br) carbons depends on the degree of debromination and the geometric structure.

	(a)	(b)	(c)	(d)	(e)	(f)
C-F (4,4')	-0.07	0.00	-0.29	-0.30	-0.08	-0.26
C-F (2,2')	0.00*	-0.14*	-0.23	-0.24	-0.25	0.00*
C-F (6,6')	0.00*	-0.14*	0.00	0.00	0.00	0.00*
C-Br	-1.25	-1.22	-1.31	-1.31	-1.15	-
C-C	-1.18	-1.91	-1.29	-1.30	-1.90	-1.15
C-Ag	-	-	-2.77	-2.79	-2.59	-2.54

Table 1 Calculated relative core-level shifts of C 1s in eV for the structures shown in Fig. 4. The carbon atom with the highest binding energy was used as reference. Core-level shifts are only given for one phenyl ring, the core-level shifts in the other phenyl ring are symmetry related. *: symmetrically equivalent

For a fully brominated and planar Br_4F_6BP monomer the C-Br BE is slightly higher than that of C-C as intuitively expected, whereas for a non-planar geometry the order is reversed with a significantly enhanced BE for C-C. In the half brominated and half organometallic compound, the BEs of C-C and C-Br are essentially similar for both planar structures, whereas for the non-planar structure C-C features a lower BE.

These simulation results in combination with additional information from Br 3d aided in fitting the C 1s peak: 35% debromination implies on average 2.4 remaining bromine substituents per molecule. Accordingly, the C-Br (with 2.4 such carbons per molecule) intensity is higher than that for the C-C species (with two such carbons per molecule). For the computationally somewhat undecided BE order of the not separately resolved C-C and C-Br species, Near-Edge X-ray Absorption Fine Structure (NEXAFS) provided additional information: The chemically distinct carbon species are also reflected as fine structure in the π*-resonance, normally even with higher sensitivity for the chemical environment of an atom than in XP Spectroscopy (XPS).[30] The strongest resonance at the highest photon energy is related to C-F with the highest C 1s BE, whereas the adjacent resonance at lower photon energies has the second strongest intensity. Hence, the C-Br BE is higher than that of C-C in agreement with the DFT results, in particular for the non-planar structure in Fig. 4(e). For fitting the XP spectra, two C-F species with slightly different BEs were considered as also suggested by the simulations. This additional information results in a good fit for C 1s as shown in Fig. 3(a) with relative amounts of 43% (50%) C-F, 25% (21.5%) C-Br, 20% (16.7%) C-C, 12.5% (12.5%) C-Ag. The values in parenthesis correspond to the percentages expected for 65% brominated sites and full conversion of 35% into organometallic sites after didebromination.

To acquire quantitative information on the phenyl tilt angles, carbon K-edge NEXAFS experiments were performed. The spectra acquired after room temperature deposition of Br_4F_6BP onto Ag(111) for five different incidence angles are depicted in Fig. 5(a). All spectra show strong C 1s → π*-resonances for photon energies below 290 eV as expected for aromatic compounds.[31-34] The fine structure consists of four resolved peaks, nicely reflecting the chemical shifts of carbon. The strongest peak at the highest photon energy of 287.7 eV corresponds to C-F with the highest C 1s BE. These results are in accord with NEXAFS spectra of a perfluorinated oligo(p-phenylene).[35] The π*-resonances exhibit a pronounced dichroism, indicating a highly uniform orientation of all molecules on the surface. A detailed analysis of the dependence of the intensity of the resonance corresponding to the phenyl-phenyl carbons on the incidence angle results in an average orientation of the transition dipole moment of (45° ± 5°) with respect to the surface (cf. Fig. 5(b)). Direct interpretation as phenyl tilt angle is not indicated, as this value appears unrealistically high. DFT simulations of the organometallic chains adsorbed on Ag(111) suggest notably
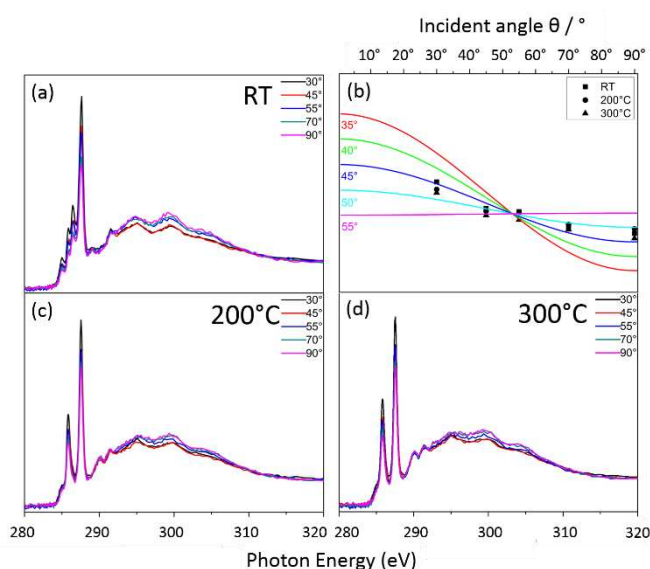

Fig. 5 Carbon K-edge NEXAFS spectra of Br_4F_6BP on Ag(111) acquired for five different incidence angles after (a) RT deposition and subsequent annealing to (c) 200 °C and (d) 300 °C. All spectra were energy- and flux-corrected, background-subtracted, and normalized. Incidence angles θ refer to the surface, i.e. 90° corresponds to normal incidence. (b) shows intensity *vs.* incidence angle θ plots for the resonance corresponding at a photon energy at 285.9 eV; the coloured solid lines are theoretical curves for the stated tilt of the transition dipole moment with respect to the surface normal, evaluated for the known X-ray polarization of P = 0.92.

smaller tilt angles, i.e. half of the dihedral angle in the biphenyl unit for a symmetric adsorption geometry, of 29° (densely packed) and 22° (loosely packed) with respect to the surface. This discrepancy could be related to more subtle effects that result in apparent tilt angles, for instance hybridization of molecular with surface electronic states or upward bending of the fluorine substituents.[36] Additionally, complications for the direct interpretation of NEXAFS data can arise from core-hole localization and π* delocalization effects in the biphenyl.[37] Perspectively, it is important to explore whether higher level NEXAFS simulations with explicit evaluation of transition dipole moments and consideration of the underlying surface result in quantitative agreement.

After sample annealing to 200 °C subsequent STM imaging revealed the coexistence of two different regular 2D networks: a flower (Fig. 2(d)) and a checkerboard structure (Fig. 2(e)) with hexagonal (a=b=(1.84±0.18) nm) and centered rectangular unit cell (a=(1.57±0.08) nm, b=(1.30±0.10) nm), respectively. In particular the flower structure exhibits a high defect density and more disordered areas or vacancies were also discerned, mainly at phase boundaries. Both ordered structures are identified as organometallic networks with C-Ag-C interlinks between fully debrominated molecules. Accordingly, the checkerboard structure features two molecules per unit cell, whereas in the flower structure each unit cell accommodates three 120° rotated molecules resulting in a structure with *p*6mm symmetry. Scaled overlays with DFT-optimized geometries perfectly match with the STM data. Accordingly, the experimental lattice parameters are consistent with optimized unit cell parameters from periodic DFT simulations with enforced planar geometry, yielding a=b=1.86 nm for the flower, and a=1.61 nm, b=1.22 nm for the

checkerboard structure, respectively. Moreover, the pronounced STM contrast of the Ag atoms in the organometallic linkages as similarly observed in comparable networks on Ag(111),[14, 18] is well reproduced in STM image simulations based on the corresponding structures (cf. ESI). Complementary experiments with 4-fold decreased heating and cooling rates (1.5 °C min⁻¹ instead of 5.8 °C min⁻¹) yielded similar results (cf. ESI). Interestingly, comparable long-range ordered organometallic structures were not observed for the topologically similar 3,5,3",5"-tetrabromo-*para*-terphenyl precursor on Cu(111).[38] A conceivable reason could be a diminished bond reversibility of the C-Cu-C linkages due to the higher organometallic bond strength.

Formation of fully cross-linked organometallic networks is triggered by progressive debromination, as also corroborated by Br 3d XP spectra indicating 86% debromination after annealing to 200 °C. Although the chemical state of the adsorbed molecules did not change markedly, the corresponding C 1s XP spectrum in Fig. 3(c) shows drastic alterations. It consists of two clearly separated main peaks, where the lowest BE peak features an additional low BE shoulder. Based on the STM results, the following assignment is proposed: the highest BE peak still corresponds to C-F. The small shoulder at the lowest BE could still be assigned to C-Ag, however, this leaves the question about the origin of the second main peak at a BE of 284.8 eV (Fig. 3(c)). STM unambiguously shows the formation of organometallic networks, which should also be reflected in XPS as increasing C-Ag intensity. To resolve this discrepancy, we propose that the second main component in C 1s can be assigned to C-Ag in fully debrominated phenyl rings within the organometallic networks (Fig. 3(c), ~284.8 eV, light pink). This implies that the chemical shift of C-Ag in the networks is ~1.24 eV smaller than that in the organometallic chains observed after room temperature deposition. This hypothesis is corroborated in the core-level shift simulations: in the half-brominated half-organometallic phenyl rings that mimic the chains, C-Ag is shifted by -2.79 eV with respect to the highest BE C-F, whereas the C-Ag shift decreases to -2.54 eV in the fully organometallic phenyl rings as in the 2D networks. Accordingly, we propose that the C-Ag shift depends on the number of organometallic bonds in the phenyl rings, with a significantly smaller BE for phenyl rings with two organometallic bonds (chains) than with four organometallic bonds (flower and checkerboard). Even though absolute values cannot be accurately reproduced by the model calculations, the trend is fully confirmed. Nevertheless, the strongest justification of our interpretation originates from the STM data, unambiguously showing organometallic networks. This interpretation is further supported by Br 3d XPS: 14% Br remained molecule-bound even after annealing to 200 °C. Assuming that all remaining Br are situated at the slightly tilted phenyl rings in the chains with one organometallic bond, this should result in 3% of the corresponding C 1s intensity, in reasonable agreement with a value of 7% from the fit. We note that this interpretation of the XPS data would not have been possible without STM data

and C 1s core level shift simulations: The chemical shift of the C-Ag species observed after annealing to 200 °C in the fully organometallically linked phenyl rings towards typical values for carbon-bound carbon could easily been misinterpreted as formation of fully covalent networks.

Further annealing to 300 °C resulted in disappearance of the checkerboard and prevalence of the flower structure as shown by the STM image in Fig. 2(f). This suggests that the flower structure is thermodynamically more stable, whereas the polymorphism observed for lower annealing temperatures of 200 °C can be attributed to kinetic effects. Even though the domain sizes increased considerably, the flower structure still exhibits a relatively high defect density. In addition, STM showed the emergence of more disordered not further resolved structures, mostly at the boundary of the remaining flower structure (Fig. 2(f) examples marked by red arrow). In XPS C 1s (Fig. 3(e)) appeared largely similar to the spectrum seen after annealing to 200 °C, only with a slight change of the intensity ratio at the expense of the C-F component. Moreover, the degree of debromination increases slightly to 91%, i.e. a safely detectable proportion of Br still remained molecule-bound (Fig. 3 (f)), whereas the total amount of Br on the surface did not change.

Further NEXAFS experiments were also carried out after annealing to 200 °C and 300 °C, respectively. The spectra depicted in Figs. 5(c) and (d) appear largely similar for both annealing temperatures. In contrast to the room temperature spectra, the shape of the π*-resonances changed from one main peak with fine structure to two peaks with comparable intensity, mirroring the changes also observed in C 1s XPS. Again an unrealistically large apparent phenyl tilt angle of (50° ± 5°) is deduced from the intensity dependence. This is at odds with the STM results, since in the 2D networks, the biphenyl units are constrained to a planar geometry by the four intermolecular organometallic bonds. As already discussed above, a straightforward interpretation of NEXAFS data assuming the transition dipole moment perpendicular to the phenyl ring is not indicated here.

Ordered organometallic networks could not be observed anymore after annealing at 400 °C. STM showed only disordered structures, where molecular units could not be discerned anymore (cf. ESI). In XPS the C 1s intensity remained constant, whereas F 1s decreased to about 75%, indicating the onset of defluorination (cf. ESI). A possible X-ray radiation damage of the fluorine functional groups appears unlikely, as an additional experiment with a 60% reduced dose showed similar results. Moreover, the total intensity of Br 3d on the surface decreased to 34% of the initial amount due to thermal desorption. The constant amount of carbon on the surface excludes sizable desorption of monomers. For such a relatively small molecule, stabilization on the surface at these high temperatures can only be achieved by forming larger aggregates, suggesting formation of covalent intermolecular

bonds. However, the lack of molecular resolution in STM may indicate more disordered structures without defined interlinks.

Discussion

Partial debromination followed by the formation of organometallic bonds is commonly observed for comparable brominated precursors on Ag(111) around room temperature.[14, 18] In this respect, the perfluorination as in Br_4F_6BP does not lead to significant changes. This is fully consistent with the expectations from our DFT-derived homolytic bond dissociation energies of C-Br bonds in the gas phase, resulting in a similar value of 4.4 eV for both Br_4F_6BP and its non-fluorinated analogue. A spectacular observation is the formation of regular 1D chains through remote site-selective didebromination at the 3- and 5'-positions. Yet, this unprecedented phenomenon can be rationalized by the interplay of bond formation between radicals and adatoms and electrostatically mediated intramolecular conformational mechanics: the first debromination occurs at a random site (referred to as 3), directly followed by formation of an organometallic bond with an Ag adatom. The relatively large difference of adsorption heights between Ag adatoms (0.236 nm in three-fold hollow sites according to the (111) lattice plane spacing or 0.244 nm according to our DFT simulations of organometallic chains) and aromatic backbones (0.316 nm for perfluoropentacene on Ag(111)[39] or 0.323 nm according to our DFT simulations of organometallic chains) tilts the first phenyl ring toward this organometallic bond. Accordingly, the adsorption height and consequently the debromination barrier of the Br at the 5-position increase, resulting in kinetic stabilization. The remote site-selective debromination at the second phenyl ring in 5'-position is mediated by the steric repulsion through the *ortho*-fluorine atoms, leading to a large dihedral angle between the two phenyl rings. This conformational tilt of the second phenyl ring in the opposite direction gives rise to a low adsorption height and debromination barrier at the 5'-position and kinetic stabilization of the Br at the 3'-position. In essence, the steric repulsion conveys the remote site-selective debromination across two phenyl rings. However, substantial differences in efficiency of this process were observed between different experimental runs: for the results shown in Fig. 2(b) overview images indicate a very high yield with almost no defects; this high regularity also enables the more dense packing of the chains; in contrast, for the results shown in Fig. 2(a) a markedly reduced selectivity of ~60% was deduced from statistical analysis of STM data (cf. ESI). Accordingly, a more subtle influence from additional preparation parameters as deposition rate and surface temperature during deposition appears likely. To shed more light on the conformational mechanics, comparative STM experiments were carried out with the non-fluorinated analogue Br_4BP. In analogy to Br_4F_6BP, room temperature deposition of Br_4BP onto Ag(111) likewise results in the formation of 1D organometallic chains (cf. ESI). These results unambiguously demonstrate that even the weaker steric repulsion of the *ortho*-hydrogens is sufficient

to mediate a site-selective 3,5'-didebromination through conformational mechanics. Interestingly, deposition of Br_4BP onto Ag(111) held at 50 °C induces high defect densities, also related to progressive dissociation of the remaining bromine substituents (cf. ESI). These additional experiments demonstrate that for Br_4BP the conformational mechanics is not very robust against higher thermal energy, hence only works in a relatively small temperature window.

The formation of organometallic networks from multiply brominated precursors on Ag(111) driven by the thermally activated progression of debromination is well documented.[14, 18, 40] In this sense, Br_4F_6BP-derived networks are a further example for "organometallic self-assembly", confirming the mandatory bond reversibility of C-Ag-C linkages. Yet, the observed polymorphism is quite uncommon for organometallic self-assembly. For Br_4F_6BP as precursor, the two experimentally observed regular structures correspond to the two least complex structures conceivable for these two-fold symmetric tectons and straight C-Ag-C linkages. Interestingly, all Ag atoms in the organometallic networks exhibit comparable apparent heights in STM, prohibiting any tilt within the biphenyl backbone. Given the large steric repulsion due to the *ortho*-fluorine atoms, co-planar adsorption appears surprising. On the other hand, DFT indicates a relatively modest energy cost of 1.32 eV for planarization of the Br_4F_6BP in the gas phase in accord with literature values.[41] The planarization is accompanied by a lengthening of the phenyl-phenyl bond from 0.1481 nm to 0.1544 nm to alleviate the electrostatic repulsion.

Even though STM indicates a largely similar adsorption height of all organometallic Ag atoms, closer inspection reveals more subtle differences: some Ag atoms appear rather noisy, whereas others could be stably imaged (examples are marked by red and green arrows, respectively, in Fig. 2(c) / (d)), ruling out tip instabilities. The distribution is not random: stable Ag atoms appear predominantly at domain boundaries and defects, whereas within the domains the majority of Ag atoms appear noisy (cf. ESI). This peculiar difference is attributed to a weakening of the surface contacts for noisy Ag atoms as a consequence of constraining the intrinsically twisted biphenyl molecules to planarity by their integration within the networks. Again, it is instructive to compare the 2D organometallic self-assembly of Br_4F_6BP and Br_4BP triggered by full debromination. In contrast to the fluorinated precursor, the non-fluorinated precursor exclusively forms the checkerboard pattern without any indications of polymorphism or the flower structure that was even the thermodynamically more stable polymorph for Br_4F_6BP (cf. ESI). Moreover, the corresponding domain sizes remain comparatively small for Br_4BP. Even though apparently related to the perfluorination, the origin of these differences is not yet clear. A possible explanation is offered by differences in surface mobility, where the inherently non-planar structure of the Br_4F_6BP precursor should give rise to a higher diffusivity. In addition, for Br_4BP large areas of the surface were covered

with densely packed domains of dissociated Br (cf. ESI), imposing serious constraints on the formation of organic networks.[42] Yet, it remains unclear as to why this halogen poisoning is more pronounced for the non-fluorinated precursor.

A further very remarkable feature of the organometallic networks derived from Br_4F_6BP is their exceptional and unprecedented thermal stability up to 300 °C. In contrast, the Br_4BP derived organometallic intermediates are converted into covalent networks upon annealing to ~200 °C (cf. ESI), in accord with hexagonal polyphenylene networks.[14] The extraordinary thermal stability of the Br_4F_6BP derived organometallic flower structure indicates high binding energies that could in principle arise either from strong molecule-molecule or strong molecule-surface interactions. However, a comparative X-ray standing wave study finds a significant enlargement of the adsorption height for perfluorinated pentacene on Ag(111), indicating a weakening of the molecule-surface interactions.[43] This suggests that the high stability of the organometallic networks here originates from strong molecule-molecule interactions as indeed rationalized by gas phase DFT simulations: planar organometallic dimers with one linear C-Ag-C linkage and three remaining Br substituents per biphenyl result in bond dissociation energies of 1.93 eV for the perfluorinated *vs.* 1.34 eV for the hydrogen-terminated dimer. Even though actual values may differ for the adsorbed system, perfluorination accounts for the extraordinary stability of the organometallic networks by increasing the C-Ag-C bond strength. By the same token, the higher bond strength restricts the reversibility, hence increases the temperatures required for structural equilibration. This may also account for both the relatively high defect densities in the organometallic networks and the relatively high temperatures required for conversion of to the metastable checkerboard into the more stable flower structure.

In contrast to other organometallic networks,[14, 18, 44] and in particular to the comparable 3,5,3",5"-tetrabromo-*para*-terphenyl precursor[45] and the non-fluorinated Br_4BP analogue, a thermally activated conversion into defined covalent networks was not observed here, not even for the highest annealing temperature of 300 °C. This is tentatively attributed to the combination of extraordinary stability of the organometallic networks, an additional barrier for covalent coupling due to the *ortho*-fluorine atoms, but also the onset of molecule degradation by defluorination at higher annealing temperatures (cf. ESI).

Conclusions

In summary, Br_4F_6BP showed a rich combination of known and unprecedented surface chemistry on Ag(111) as summarized in Fig. 1: While formation and equilibration of organometallic structures is meanwhile well established, the formation of defined 1D organometallic chains for both the fourfold

brominated perfluorinated Br_4F_6BP and non-fluorinated Br_4BP precursor is unique. This chain formation involves the regioselective activation of only two out of the precursor's four active sites. This is explained by a remote site-selective 3,5'-didebromination, mediated across the biphenyl unit by its conformational non-planarity due to the intramolecular repulsion of either the *ortho*-fluorine or *ortho*-hydrogen substituents. This constitutes an instructive and highly useful example of conformational mechanics in on-surface synthesis: formation of chemical bonds with the surface upon activation of specific sites of a molecular entity is accompanied by an increase of adsorption height, and hence deactivation at the opposing sites. The proposed symmetry breaking mechanism has broader implications for on-surface synthesis as it provides a rationale for the observed stepwise or uncommonly gradual and selective activation in apparently symmetric monomers.[14, 18] In this respect, it is intriguing that already the significantly weaker steric hindrance in the non-fluorinated Br_4BP precursor is sufficient to drive this conformational mechanics.

In contrast, both the polymorphism and the exceptional stability of organometallic networks are unique observations for the Br_4F_6BP precursor. As indicated by our DFT simulations, the perfluorination can be held responsible for the high stability of the organometallic networks. Even though it decreases the adsorption energy of aromatic molecules on metals, by the same token the strength of intermolecular C-Ag-C linkages is markedly enhanced. The exceptional strength of the intermolecular organometallic bonds is even sufficient to overcome the large electrostatic repulsion within the molecules and incorporate them in into extended 2D networks. Yet, the role of the perfluorination for the polymorphism remains unclear. Tentatively, either the enhanced surface mobility of Br_4F_6BP due to the non-planar structure or the large amounts of adsorbed bromine for Br_4BP could be held responsible and would also be consistent with the larger domain sizes observed for Br_4F_6BP as compared to Br_4BP.

Interestingly, as already indicated by DFT-derived C-Br bond dissociation energies, there is no pronounced effect of the perfluorination on the debromination barrier, as debromination temperatures are within the typical range reported for non-fluorinated precursors.[14, 18] Accordingly, in terms of activation, perfluorinated monomers are equally suitable for debrominative coupling on surfaces. Yet, covalent coupling into defined structures as templated by the organometallic flower structure remains elusive for Br_4F_6BP on Ag(111). This is an important finding as it provides valuable guidelines for the design of fluorinated monomers suitable for covalent aryl-aryl coupling, for instance by combining *ortho*-fluorine with *ortho*-hydrogen substitution. Alternatively, the substantially increased intermolecular bond strength in the organometallic networks derived from perfluorinated precursors provides a perspective for directly using the highly stable organometallic 2D polymers for improved structural quality.

Materials and Methods

All STM, NEXAFS, and XPS experiments were carried out under ultrahigh vacuum (UHV) conditions with base pressures below 3×10^{-10} mbar (STM) and 8×10^{-10} mbar (XPS, NEXAFS). Ag(111) single crystals surfaces were prepared by cycles of 0.5 keV-Ar^+ sputtering and annealing at 500 °C. 3,3',5,5'-tetrabromo-2,2',4,4',6,6'-hexafluorobiphenyl (Br_4F_6BP) was synthesized according to literature procedures[46, 47] (cf. ESI) and deposited by sublimation from a home-built Knudsen-cell with crucible temperatures between 55 °C and 80 °C at a pressure of 3×10^{-9} mbar.[48] The non-fluorinated analogue 3,3',5,5'-tetrabromo-1,1'-biphenyl (Br_4BP) was purchased from Sigma Aldrich (≤100% purity). Its vapour pressure at room temperature is high enough to facilitate deposition from a Knudsen-cell without additionally heating the crucible. STM data were recorded at room temperature with a home-built microscope controlled by an SPM100 controller (RHK Technology Inc.). NEXAFS and XPS measurements were carried out in a Prevac endstation at the HE-SGM beamline at Helmholtz-Zentrum Berlin. NEXAFS carbon K-edge spectra were acquired in the analysis chamber using a home-built double channel plate detector in partial electron yield mode (U= -150V). XP spectra of C 1s, Br 3d, and F 1s were measured with a Scienta R3000 electron analyzer at normal electron emission with a pass energy of 50 eV. Photon energies of 450 eV for C 1s and Br 3d and 750 eV for F 1s were used, respectively. For energy calibration a Ag $3d_{5/2}$ binding energy of 368.2 eV was used as internal standard.[49]

Dispersion-corrected DFT simulations were performed either with periodic boundary conditions (organometallic chains, flower and checkerboard structure) or for isolated molecules (C 1s core-level shifts) with the FHI-aims computing package.[50] Geometry optimizations for the unit cells containing one (organometallic chains and checkerboard structure) or three (flower structure) molecules with two (organometallic chains) and four (checkerboard and flower structure) Br atoms exchanged for Ag were performed with FHI-aims at "tight" computational settings, 4×4×1 k-point sampling, and using a 30 Å vacuum region. In these calculations electronic exchange and correlation (xc) was treated on the generalized-gradient approximation level with the PBE functional,[51] augmented by dispersive interactions through the Tkatchenko-Scheffler TSsurf method.[52] All structures were fully relaxed until residual forces were below 10 meV/Å. The adsorbed organometallic chains were optimized on Ag(111) slabs with 11 and 15 atoms per layer. A lattice parameter of a_{Ag} = 4.152 Å was used and the first of two layers were allowed to relax. The influence of the weakly interacting Ag(111) surface was neglected in the simulations of the 2D flower and checkerboard structures, but the unit cell size was optimized together with the geometry. STM image simulations were performed based on the DFT-optimized structures according to the Tersoff-Hamann approach.[53] Therefore, all electronic states in an energy window defined by the bias voltage and the Fermi energy were summed to produce the final image. C 1s core-level energies

were calculated with a 1s core-hole on each symmetry-inequivalent carbon atom one at a time. The maximum overlap method was used to prevent variational collapse to the ground state.[54, 55]

Conflicts of interest

There are no conflicts to declare.

Acknowledgements

Notes and references

1. J. V. Barth, G. Costantini and K. Kern, *Nature*, 2005, **437**, 671-679.
2. J. V. Barth, *Annu. Rev. Phys. Chem.*, 2007, **58**, 375-407.
3. D. F. Perepichka and F. Rosei, *Science*, 2009, **323**, 216-217.
4. L. Dong, Z. A. Gao and N. Lin, *Prog Surf Sci*, 2016, **91**, 101-135.
5. J. Eichhorn, D. Nieckarz, O. Ochs, D. Samanta, M. Schmittel, P. J. Szabelski and M. Lackinger, *ACS Nano*, 2014, **8**, 7880-7889.
6. W. Z. Yuan, X. Y. Shen, H. Zhao, J. W. Y. Lam, L. Tang, P. Lu, C. Wang, Y. Liu, Z. Wang, Q. Zheng, J. Z. Sun, Y. Ma and B. Z. Tang, *J. Phys. Chem. C*, 2010, **114**, 6090-6099.
7. B. Wurster, D. Grumelli, D. Hötger, R. Gutzler and K. Kern, *J. Am. Chem. Soc.*, 2016, **138**, 3623-3626.
8. R. Gutzler, S. Stepanow, D. Grumelli, M. Lingenfelder and K. Kern, *Acc. Chem. Res.*, 2015, **48**, 2132-2139.
9. J. I. Urgel, D. Écija, G. Lyu, R. Zhang, C.-A. Palma, W. Auwärter, N. Lin and J. V. Barth, *Nat. Chem.*, 2016, **8**, 657-662.
10. M. D. Giovannantonio and G. Contini, *J. Phys.: Condens. Matter*, 2018, **30**, 093001.
11. C. J. Judd, S. L. Haddow, N. R. Champness and A. Saywell, *Sci. Rep.*, 2017, **7**, 14541.
12. M. Ammon, T. Sander and S. Maier, *J. Am. Chem. Soc.*, 2017, **139**, 12976-12984.
13. Q. Sun, L. Cai, H. Ma, C. Yuan and W. Xu, *ACS Nano*, 2016, **10**, 7023-7030.
14. J. Eichhorn, T. Strunskus, A. Rastgoo-Lahrood, D. Samanta, M. Schmittel and M. Lackinger, *Chem. Commun.*, 2014, **50**, 7680-7862.
15. Z. Chen, C. Molina-Jirón, S. Klyatskaya, F. Klappenberger and M. Ruben, *Ann. Phys.*, 2017, **529**, 1700056.
16. Q. Shen, H.-Y. Gao and H. Fuchs, *Nano Today*, 2017, **13**, 77-96.
17. M. Lackinger, *Chem. Commun.*, 2017, **53**, 7872-7885.

18. R. Gutzler, L. Cardenas, J. Lipton-Duffin, M. E. Garah, L. E. Dinca, C. E. Szakacs, C. Fu, M. Gallagher, M. Vondráček, M. Rybachuk, D. F. Perepichka and F. Rosei, *Nanoscale*, 2014, **6**, 2660-2668.
19. G. Kuang, S. Z. Chen, L. Yan, K. Q. Chen, X. Shang, P. N. Liu and N. Lin, *J. Am. Chem. Soc.*, 2018, **140**, 570-573.
20. P. Wagner, C. P. Ewels, J.-J. Adjizian, L. Magaud, P. Pochet, S. Roche, A. Lopez-Bezanilla, V. V. Ivanovskaya, A. Yaya, M. Rayson, P. Briddon and B. Humbert, *J. Phys. Chem. C*, 2013, **117**, 26790-26796.
21. D. Gunlycke, J. Li, J. W. Mintmire and C. T. White, *Nano Lett.*, 2010, **10**, 3638-3642.
22. H. Hayashi, J. Yamaguchi, H. Jippo, R. Hayashi, N. Aratani, M. Ohfuchi, S. Sato and H. Yamada, *ACS Nano*, 2017, **11**, 6204-6210.
23. C. Schmidt, T. Breuer, S. Wippermann, W. G. Schmidt and G. Witte, *J. Chem. Phys. C*, 2012, **116**, 24098-24106.
24. K. E. Riley, J. S. Murray, J. Fanfrlík, J. Řezáč, R. J. Solá, M. C. Concha, F. M. Ramos and P. Politzer, *J. Mol. Model.*, 2011, **17**, 3309-3318.
25. S. Kawai, A. Sadeghi, F. Xu, L. Peng, A. Orita, J. Otera, S. Goedecker and E. Meyer, *ACS Nano*, 2015, **9**, 2574-2583.
26. M. Smerieri, I. Píš, L. Ferrighi, S. Nappini, A. Lusuan, C. D. Valentin, L. Vaghi, A. Papagni, M. Cattelan, S. Agnoli, E. Magnano, F. Bondino and L. Savio, *Nanoscale*, 2016, **8**, 17843-17853.
27. I. Píš, L. Ferrighi, T. H. Nguyen, S. Nappini, L. Vaghi, A. Basagni, E. Magnano, A. Papagni, F. Sedona, C. D. Valentin, S. Agnoli and F. Bondino, *J. Chem. Phys. C*, 2016, **120**, 4909-4918.
28. D. T. Clark, D. Kilcast and W. K. R. Musgrave, *J. Chem. Soc. D*, 1971, **0**, 516b-518.
29. D. T. Clark, D. Kilcast, D. B. Adams and W. K. R. Musgrave, *J. Electron Spectrosc. Relat. Phenom.*, 1972, **1**, 227 - 250.
30. G. Hähner, *Chem. Soc. Rev.*, 2006, **35**, 1244-1255.
31. K. H. Frank, P. Yannoulis, R. Dudde and E. E. Koch, *J. Chem. Phys.*, 1988, **89**, 7569-7576.
32. H. Oji, R. Mitsumoto, E. Ito, H. Ishii, Y. Ouchi, K. Seki, T. Yokoyama, T. Ohta and N. Kosugi, *J. Chem. Phys.*, 1998, **109**, 10409-10418.
33. K. Hänel, S. Söhnchen, S. Lukas, G. Beernik, A. Birkner, T. Strunskus, G. Witte and C. Wöll, *J. Mater. Res.*, 2004, **19**, 2049-2056.
34. S. Söhnchen, S. Lukas and G. Witte, *J. Chem. Phys.*, 2004, **121**, 525-534.
35. K. K. Okudaira, K. Ohara, H. Setoyama, T. Suzuki, Y. Sakamoto, M. Imamura, S. Hasegawa, K. Mase and N. Ueno, *Nucl. Instr. Meth. Phys. Res.*, 2003, **199**, 265-269
36. C. Mainka, P. S. Bagus, A. Schertel, T. Strunskus, M. Grunze and C. Wöll, *Surf. Sci.*, 1995, **341**, L1055-L1060.
37. M. G. Ramsey, F. P. Netzer, D. Steinmüller, D. Steinmüller-Nethl and D. R. Lloyd, *J. Chem. Phys.*, 1992, **97**, 4489-4495.
38. Q. Fan, C. Wang, L. Liu, Y. Han, J. Zhao, J. Zhu, J. Kuttner, G. Hilt and J. M. Gottfried, *J. Phys. Chem. C*, 2014, **118**, 13018-13025.
39. S. Duhm, S. Hosoumi, I. Salzmann, A. Gerlach, M. Oehzelt, B. Wedl, T.-L. Lee, F. Schreiber, N. Koch, N. Ueno and S. Kera, *Phys. Rev. B*, 2010, **81**, 045418.
40. M. Bieri, S. Blankenburg, M. Kivala, C. A. Pignedoli, P. Ruffieux, K. Müllen and R. Fasel, *Chem. Commun.*, 2011, **47**, 10239.
41. F. Grein, *J. Chem. Phys. A*, 2002, **106**, 3823-3827.
42. S. Schlögl, W. M. Heckl and M. Lackinger, *Surf. Sci.*, 2012, **606**, 999-1104.
43. N. Koch, A. Gerlach, S. Duhm, H. Glowatzki, G. Heimel, A. Vollmer, Y. Sakamoto, T. Suzuki, J. Zegenhagen, J. P. Rabe and F. Schreiber, *J. Am. Chem. Soc.*, 2008, **130**, 7300-7304.
44. J. P. Beggan, N. M. Boyle, M. T. Pryce and A. A. Cafolla, *Nanotechnology*, 2015, **26**, 365602.
45. J. Dai, Q. Fan, T. Wang, J. Kuttner, G. Hilt, J. M. Gottfried and J. Zhu, *Phys. Chem. Chem. Phys.*, 2016, **18**, 20627-20634.
46. Y. Sakamoto, T. Suzuki, A. Miura, H. Fujikawa, S. Tokito and Y. Taga, *J. Am. Chem. Soc.*, 2000, **122**, 1832-1833.
47. F. Leroux, R. Simon and N. Nicod, *Lett. Org. Chem.*, 2006, **3**, 948-954.
48. R. Gutzler, W. M. Heckl and M. Lackinger, *Rev. Sci. Instrum.*, 2010, **81**, 015108.
49. G. Johansson, J. Hedman, A. Berndtsson, M. Klasson and R. Nilsson, *J. Electron Spectrosc. Relat. Phenom.*, 1973, **2**, 295-317.
50. V. Blum, R. Gehrke, F. Hanke, P. Havu, V. Havu, X. Ren, K. Reuter and M. Scheffler, *Comput. Phys. Commun.*, 2009, **180**, 2175-2196.
51. J. P. Perdew, K. Burke and M. Ernzerhof, *Phys. Rev. Lett.*, 1996, **77**, 3865-3868.
52. V. G. Ruiz, W. Liu, E. Zojer, M. Scheffler and A. Tkatchenko, *Phys. Rev. Lett.*, 2012, **108**, 146103.
53. J. Tersoff and D. R. Hamann, *Phys. Rev. B*, 1985, **31**, 805-813.
54. N. A. Besley, A. T. B. Gilbert and P. M. W. Gill, *J. Chem. Phys*, 2009, **130**, 124308.
55. A. T. B. Gilbert, N. A. Besley and P. M. W. Gill, *J. Phys. Chem. A*, 2008, **112**, 13164-13171.